

# **Modelling the Photoelectron Angular Distributions of Molecular Anions: The Role of Basis Set, Orbital Choice, and Geometry**

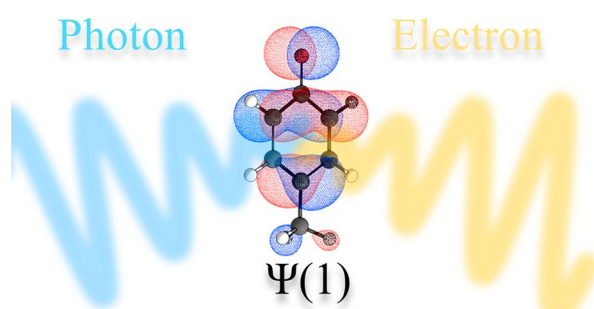
*Cate S. Anstöter<sup>[a,b]</sup>\* and Jan R. R. Verlet<sup>[b]</sup>*

[a] Present Address: Department of Chemistry, Temple University, Philadelphia, PA, 19121, USA

[b] Department of Chemistry, Durham University, DH1 3LE, United Kingdom

**ABSTRACT:** A study investigating the effect of the basis set, orbital choice, and geometry on the modelling of photoelectron angular distributions (PADs) of molecular anions is presented. Experimental and modelled PADs for a number of molecular anions, including both closed and open-shell systems, are considered. Guidelines are suggested for chemists who wish to design calculations to capture the correct chemical physics of the anisotropy of photodetachment, while balancing the computational cost associated with larger molecular anions.

## TOC GRAPHICS



**KEYWORDS** Photoelectron angular distributions, Anion photoelectron spectroscopy, Dyson orbitals, Canonical Orbitals

## Introduction

Photoelectron imaging of anions is a powerful tool, able to probe the electronic structure and dynamics of anions.<sup>1-3</sup> There is a wealth of sophisticated studies that utilise this approach to unravel the intrinsic dynamics of anions in the gas phase.<sup>4-17</sup> However, many of these studies have relied on the interpretation of the kinetic energy spectrum in isolation, often overlooking the insight offered by the complementary angular components of the photodetached electron.

The angular distribution of photoelectrons produced in a single-photon process by linear polarised light has the general form<sup>18</sup>

$$I(\theta) = \frac{\sigma}{4\pi} (1 + \beta_2 P_2 \cos(\theta)),$$

where  $\theta$  is the angle of the ejected photoelectron relative to the polarisation axis of light,  $\sigma$  is the total photodetachment cross section,  $P_2 \cos(\theta)$  is the second-order Legendre polynomial, and  $\beta_2$  is the anisotropy parameter. The  $\beta_2$  parameter is constrained between the bounds of +2 and -1 and contains important information about the angular momentum of the photoelectron, and by extension the molecular orbital (MO) from which the photoelectron was ejected.<sup>19</sup> Qualitatively, low-energy (less than a few eV) photoelectrons with anisotropy parallel to the laser (positive  $\beta_2$  values) are attributed to have originated from MOs with  $\sigma$ -character, while perpendicular anisotropy (negative  $\beta_2$  values) arises from MOs with  $\pi$ -character.<sup>20</sup>

Unravelling the information contained in the photoelectron angular distributions (PADs) has lagged behind the information content of the spectra, in part due to the necessity for quantitative computational models. The experimental  $\beta_2$  parameter inherently contains information about the electronic structure and dynamics of the system the photoelectron is ejected from.<sup>11,20,21</sup> It is desirable to be able to quantitatively or qualitatively model and interpret the complementary information encoded in the PADs. Cooper and Zare developed a formalism to predict  $\beta_2$  for atomic systems using a partial wave expansion of the outgoing electrons.<sup>18</sup> Extending this to molecular systems, Sanov *et al.* developed a non-perturbative

model for predicting the energy dependent photoelectron angular distributions of molecular anions from a mixed sp-state, based on symmetry arguments.<sup>22</sup> For molecular anions,  $l$  is not a good quantum number as it is for atomic anions. Nevertheless, in some cases, molecular orbitals may be approximated to atomic s-, p- or d-like functions and  $l$  is a good quantum number. However, in general, a single value of  $l$  is not sufficient. Instead, a superposition of two or more atomic-like orbitals offers a better approximation. The net observed photoelectron angular distribution from the s-p mixed model is a superposition of the distributions. Sanov's s-p model has been very successful in predicting the energy dependence of PADs in small molecular systems.<sup>23,24</sup> It has also recently been extended to account for d-states<sup>25</sup> and applied to non-valence states.<sup>26</sup> However, modelling the parent orbital as a linear combination of s- and p-states becomes less rigorous for large molecular systems.

In the quest to quantitatively predict the PADs for larger molecular anions, the use of *ab initio* calculations should offer an excellent starting point as it generally can predict with good accuracy the electronic structure of the anion and, hence, by extension, should be able to accurately model the PADs. A flexible and powerful framework for computing photoionisation of not only ground, but also open-shell and excited states, is the equation-of-motion coupled cluster (EOM-XX-CCSD) formalism.<sup>27-30</sup> This electronic structure method allows the calculation of the Dyson orbital to model the PADs as a function of energy for a specific photodetachment channel. Conceptually, Dyson orbitals can be thought of as the one-electron wavefunction of the leaving electron, before photodetachment.<sup>31-33</sup> For an anionic system, the Dyson orbital,  $\Psi_{\text{Dyson}}(1)$ , represents the overlap between an  $N$  electron molecular wavefunction and the  $N^{-1}$  electron wavefunction of the corresponding neutral,

$$\Psi_{\text{Dyson}}(1) = \sqrt{N} \int \Psi_i^N(1, \dots, n) \int \Psi_f^{N-1}(2, \dots, n) d2 \dots dn,$$

where  $i$  and  $f$  refer to the initial and final states, respectively. As such, the MO from which the outgoing electron is ejected provides a good approximation of the Dyson orbital. At this

point, it is worth noting that, for modelling the PADs with the Dyson orbital approach, the initial and final states are not restricted to be the ground electronic state of the respective systems, so long as the difference in electronic state can be accurately described by a single electron. For example, detachment channels from the ground electronic state of the anion to excited states of the neutral can still be represented with a single electronic transition, and therefore the Dyson orbital approach. The Dyson orbital is rigorous and accounts for the electronic relaxation in the final state upon photodetachment (see Equation 1). However, if the detachment process only involves a single electron, then the electronic relaxation is often small and may be ignored. In such cases, one can approximate the Dyson orbital by the canonical MO from which the electron is detached, which in turn offers the opportunity to employ much less expensive computational methods.

The PADs can be modelled through calculation of the transition dipole moment between the Dyson (or canonical) orbital and the final (continuum) state of the ejected electron,  $\Psi_k^{el}$ , with appropriate averaging of the molecular frame.<sup>28,34</sup> This is achieved through calculation of the photoelectron dipole matrix element,  $D_k^{if}$ ,

$$D_k^{if} = \boldsymbol{\varepsilon} \langle \Psi_{\text{Dyson}}(1) | \hat{\mathbf{r}} | \Psi_k^{el} \rangle$$

where  $k$  is the magnitude of the photoelectron wave vector  $\mathbf{k}$ ,  $\hat{\mathbf{r}}$  is the dipole moment operator and  $\boldsymbol{\varepsilon}$  is a unit vector in the direction of the polarisation of light.

This paper aims to explore the applicability of using Dyson and canonical orbitals to model the PADs for direct detachment channels between ground anion to ground neutral and ground anion to neutral-excited electronic states. There has been an abundance of promising work demonstrating the strength of the Dyson orbital approach in reproducing experimental observables.<sup>35-45</sup> In order to provide guidelines for important parameters to consider when designing calculations to model the PADs of molecular anions, we have chosen to use three systems which encompass a number of different electron loss channels and physical

properties. The three molecular anions studied consist of two closed-shell systems, para-methyl and para-vinyl phenolate, and one open-shell system, the  $\text{SO}_3$  monoanion. The para-substituted phenolates have two experimentally probed direct detachment channels, the ground-to-ground state  $\text{S}_0 + h\nu \rightarrow \text{D}_0 + \text{e}^-$ , and the ground-to-neutral-excited state channels  $\text{S}_0 + h\nu \rightarrow \text{D}_1 + \text{e}^-$ ,  $\text{D}_0$  and  $\text{D}_1$  channels, respectively. The  $\text{SO}_3$  anion has a single ground-to-ground state channel  $\text{D}_0 + h\nu \rightarrow \text{S}_1 + \text{e}^-$ , the  $\text{S}_0$  channel. The relevant computed Dyson orbitals for the three channels are shown in Figure 1.

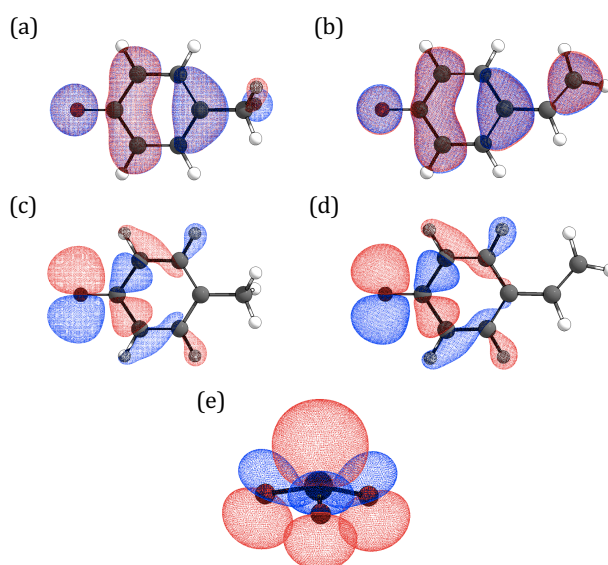


Figure 1. Representation of the Dyson orbitals for both the  $\text{D}_0$  and  $\text{D}_1$  direct detachment channel of para-methyl phenolate, (a) and (c) respectively, and para-vinyl phenolate, (b) and (d) respectively, and (e) the  $\text{S}_0$  direct detachment channel of the  $\text{SO}_3$  monoanion.

Here, we present a benchmark study demonstrating the key physical parameters that should be considered when designing calculations to model the PADs of anions. We note that this study solely explores the quality of the description of the Dyson or approximate canonical orbital and how this affects the modelled PADs, through the level of theory used in the orbital description, and consideration of experimental effects on discrepancies between the modelled and observed PADs. That is to say, we focus on the choices made in the electronic structure calculation of the orbital, rather than any choices made in the how the orbital is used to obtain

the PADs. For the latter, we use the ezDyson package<sup>46</sup> and we do not offer any discussion on the operation and tuning of parameters using ezDyson, nor do we make any comment on the assumptions made in the ezDyson program itself. Rather we direct the reader to a number of excellent papers that discuss these considerations.<sup>27,28,47-49</sup>

## Methods

The experimental PADs have been previously published and a discussion of the experimental set-up and data processing methods can be found there.<sup>40,50</sup> The absolute errors with the experimental  $\beta_2$  values are on the order of  $\pm 0.1$ , however, relative  $\beta_2$  values are often more accurate.

The geometries of the  $\text{SO}_3$  monoanion and neutral were optimised with the CCSD method using the aug-cc-pVTZ basis set and confirmed to be stationary points on the potential energy surfaces by vibrational analysis at the same level of theory. The anion and neutral geometries for both para-phenolate systems were optimised at the MP2/aug-cc-pVDZ level of theory and confirmed to be stationary points with the same level of theory. All electronic structure calculations were performed using the QChem 5.3 computational package,<sup>51</sup> unless stated otherwise.

Using the equilibrium geometries of the respective anions, the description of the orbital was explored through calculation of orbital densities with different methods and different basis sets. Hartree-Fock (HF) and density functional theory (DFT) canonical orbitals and EOM-IP-CCSD Dyson orbitals were used for all molecular anions, with the aug-cc-pVTZ basis set. Three different DFT functionals, (B3LYP, CAM-B3LYP and PBE0)<sup>52-54</sup> were chosen. The EOM-EA-CCSD Dyson orbital for the  $\text{SO}_3$  monoanion was considered and details are given in the SI (Figure SI1).

The basis set used to describe the orbital densities were investigated using B3LYP for all molecular anions. The effect of inclusion of diffuse and polarisation functions on the PADs was modelled using the Pople and Dunning families of basis sets.<sup>55,56</sup> For the former the 6-31G, 6-31G\*\*, 6-31++G and 6-31++G\*\* basis sets were used and for the latter, cc-pVDZ, cc-pVTZ, aug-cc-pVDZ and aug-cc-pVTZ.

To evaluate the effect of geometry on the PADs, 10 sample geometries, displaced from the equilibrium geometry, were calculated using a temperature defined Wigner distribution using the Newton-X computational program.<sup>57,58</sup> This procedure was carried out at 200 K, 300 K, 400 K, 500 K and 600 K. For each temperature, the PADs were modelled using all displaced geometries, and an average, assuming the total cross-section is the same, was taken. The canonical orbitals were calculated using B3LYP/aug-cc-pVTZ for all molecular anions.

All simulated PADs were modelled using the ezDyson 3.0 computational program,<sup>46</sup> developed by Krylov and Gozem.<sup>49</sup> All ezDyson calculations used the plane wave approximation to describe the continuum state of the photoelectron, and numerical averaging over molecular orientations.

## **Results and Discussion**

Before delving into the results and discussion, it is prudent to first make some overarching statements to the intended audiences. For experimentalists, it is important to appreciate that the modelling of any experimental observable depends on whether qualitative or quantitative results are required. This choice shapes the design of the calculation that will allow the modelling of the observable for the correct physical reasons. For theoreticians, it is important to consider experimental conditions, to ensure that any discrepancies between the modelled and experimental data can be balanced and rationalised. For both groups, anions provide a somewhat poorly behaved class of molecules, often not best represented by the most commonly

available electronic structure methods. The purpose of this paper is to illuminate some of the common pitfalls and highlight routes that can be taken to ensure physically meaningful modelled PADs of larger molecular anions can be obtained.

### ***Orbital Choice***

The choice of orbital intuitively represents an important parameter for modelling the PADs of a molecular anion. The Dyson orbital approach obtains an accurate description of the 1-electron wavefunction of the ejected electron through the elegant EOM-XX-CCSD methods.<sup>27,28</sup> While this is a mathematically rigorous way to ensure the correct physics of the outgoing photodetached electron, these methods become expensive for larger molecular anions.

When considering larger molecular anions, it becomes attractive to consider using less costly methods to obtain a molecular orbital that can be approximated for the Dyson orbital. Two such methods include HF and DFT. Both of these methods are considered with respect to the ‘gold standard’ EOM-XX-CCSD Dyson orbital.

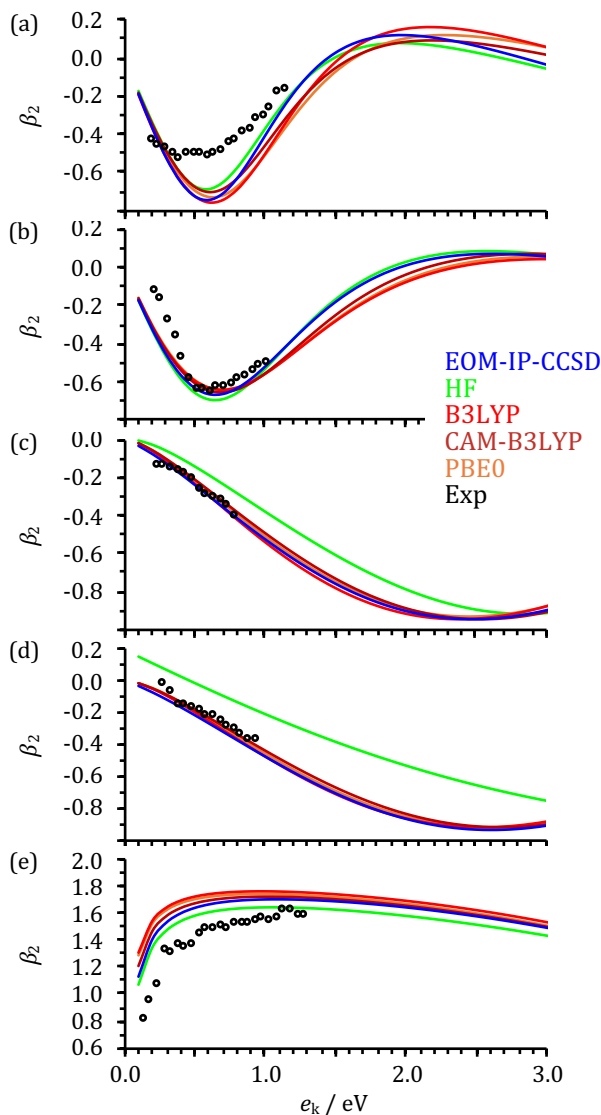


Figure 2 The effect of orbital choice on the modelled PADs for the  $D_0$  channel of para-methyl phenolate (a) and para-vinyl phenolate (b), the  $D_1$  channel of para-methyl phenolate (c) and para-vinyl phenolate (d) and the  $S_0$  channel of the  $SO_3$  anion (e). Legend is shown inset. Experimental data can be found in references 40 and 50.

Figure 2 illustrates the agreement between experimental and modelled PADs for the direct detachment channels defined by the Dyson orbitals in Figure 1. For all systems and all choices of orbitals there is good qualitative agreement between the experimental and modelled PADs. While it may appear at first to be a general insensitivity to the MO used to represent the detachment channel, there are some general lessons to be learnt from the findings.

The  $D_0$  channel of para-methyl and para-vinyl phenolate (Figure 2(a) and (b), respectively) show very good qualitative agreement between the trends for all methods and experiment for

$e_k < 1$  eV. At higher energy, the experimental data becomes unmeaningful due to the onset of resonances. At these higher energies the qualitative trends between modelled PADs are similar although there are minor quantitative deviations. The  $D_1$  channel shows different dependencies on the orbital choice. For both the para-methyl and para-vinyl phenolate, Figure 2(c) and (d), respectively, excellent quantitative agreement between the experimental data and the modelled data for the DFT canonical orbitals and the Dyson orbital. However, a clear deviation in trend is seen for the HF orbital. For both systems the change in behaviour is the same, specifically the HF orbital deviates from quantitative agreement for the PADs, with consistently underestimated anisotropies.

The  $S_0$  channel of the open-shell  $SO_3$  anion, Figure 2(e), shows similar orbital sensitivities as the  $D_1$  channel of the para-phenolates. The absolute magnitude of the anisotropy is lowered by the use of an HF orbital, and raised by the use of a DFT orbital, relative to the EOM-IP-CCSD Dyson orbital. Unlike the para-phenolate channels, in which deviations in modelled PADs become pronounced at  $e_k > 1$  eV, the offset between PADs modelled with different orbitals are consistently independent of increasing  $e_k$  for the  $SO_3$  anion. We note that the overall agreement between the experimental and modelled PADs is worse for the  $S_0$  channel of the  $SO_3$  anion. As this system is openshell, we considered that this discrepancy may arise from the reference doublet wavefunction used in the EOM-IP-CCSD Dyson orbital calculation. We ran a further EOM-EA-CCSD calculation, using the closed-shell singlet reference wavefunction of the neutral to obtain the Dyson orbital for this detachment channel. As has been previously seen for small systems,<sup>59</sup> the choice of EOM-EA or EOM-IP did not lead to meaningful changes in the description of the physical properties (see Figure SI1). We note that this consideration could become important as the size of molecular anions increases.

The results presented give compelling evidence for the use of HF or DFT canonical orbitals to model the PADs of larger molecular anions. However, one should be cautious of using HF

or DFT orbitals for systems for which the respective methods are known to perform poorly. For cases such as the  $D_0$  channel of the para-phenolates, the initial molecular anions are closed-shell that can be considered to be well-behaved with respect to electronic structure methods. That is to say, the ground-state wavefunction is dominated by a single electronic configuration and, as such, an adequate description of the canonical orbital may be obtained with conventional methods, such as HF or DFT. However, the  $D_1$  channel of the para-phenolates and the  $S_0$  channel of the  $SO_3$  anion provide more cantankerous examples of electronic structure, for which the description of the canonical orbital by HF is found to underestimate the anisotropy in the modelled PADs. For electron loss channels of excited states and open-shell systems, for which multiconfigurational wavefunctions are needed, the shape of the orbital is more sensitive. For such cases we would advise caution in using less rigorously defined canonical orbitals, and instead use Dyson orbitals.

### ***Basis Set Choice***

The computational cost of full EOM-XX-CCSD calculations of the Dyson orbital increase with size not just due to the method, but also because of the basis set required to capture the electron correlation and polarizability of molecular anions. We recommend abstaining from the temptation to decrease computational cost through reduction of the basis set. On the face of it, basis set reduction may seem like a reasonable route to scale up to larger molecular sizes, however, it should be noted that both the method and basis set chosen to describe the orbital density should be balanced. There is very little merit to using a high accuracy method with a restricted basis set.

In this study, we use the Pople and Dunning family of basis sets, the former for their perennial popularity and the latter for their ability to accurately capture physical properties of

anions. For all molecular anions, the effect of diffuse functions and polarization functions on the description of the canonical orbital and therefore the PADs, were explored.

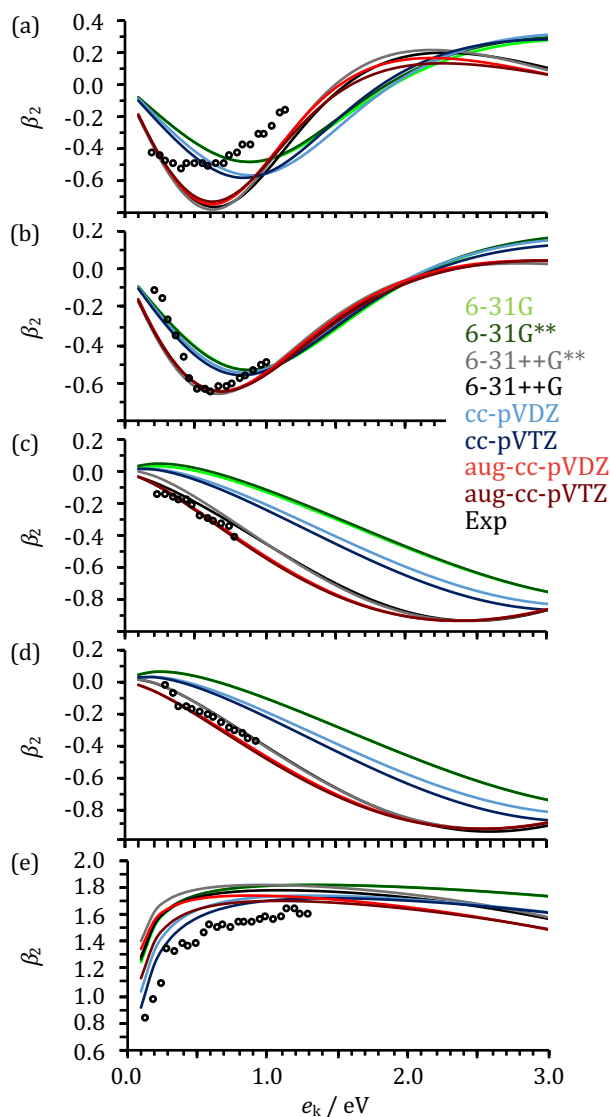


Figure 3 The effect of basis set choice on the modelled PADs for the  $D_0$  channel of para-methyl phenolate (a) and para-vinyl phenolate (b), the  $D_1$  channel of para-methyl phenolate (c) and para-vinyl phenolate (d) and the  $S_0$  channel of the  $SO_3$  anion (e). Legend is shown inset.

The sensitivity of the canonical orbital to the basis set is starkly obvious from Figure 3. For both direct detachment channels for the para-phenolates, Figure 3(a) - (d), the dependencies are the same despite the changing character of orbital. A clear quantitative agreement can be seen between the experimental data and basis sets that include diffuse functions (+ and aug-,

for the Pople and Dunning basis sets, respectively). In contrast, poor quantitative agreement is seen for basis sets that do not include diffuse functions, while some qualitative reproduction of the experimental trends is preserved. For the modelled PADs shown in Figure 3(a) - (d), the values of  $\beta_2$  are less anisotropic for basis sets without diffuse functions. A far smaller dependency can be seen for the inclusion of polarisation functions (\*) and the value of the zeta component, for the Pople and Dunning basis sets, respectively).

The results for the open-shell  $\text{SO}_3$  anion, Figure 3(e), show a rather different story. In this case, the orbital shows a greater sensitivity to the family of basis sets used, with the Pople basis sets giving more anisotropic values than the Dunning basis set. For the latter family, a larger dependence is seen regarding the polarisation functions included, with significant differences in the modelled anisotropies between cc-pVDZ and cc-pVTZ.

It is our recommendation that any compromises to the size of basis set should only involve the polarisation functions, for well-behaved closed-shell systems. For the open-shell system considered here, the advice is less clear cut; it appears that care should be taken to include both polarisation and diffuse functions to achieve a balanced description of the orbital density.

### ***Experimental Considerations***

As highlighted at the beginning of the results and discussion, the design of a calculation to model experimental parameters should consider the experimental conditions. All of the experimental results presented here were taken on a gas phase photoelectron spectrometer with an electrospray ionisation source, where anions are at a temperature defined by the trapping conditions in the instrument. In the cases presented here, this is around 300 K.

Minimum energy structures do not account for geometric displacements that may occur due to internal temperatures of the anions. That is to say, there is enough energy to cause displacements away from the minimum energy structure and, whilst generally considered to be

small, these geometric perturbations can affect the electronic structure of the anion as very clearly demonstrated in our previous work on para-ethyl phenolate,<sup>40</sup> where torsion about the ethyl carbon atoms alters the Dyson orbital to such an extent that  $\beta_2$  parameters change from negative to positive for in-plane ethyl to out-of-plane ethyl, respectively.

There is of course nuance, a given thermodynamic temperature will impact the distribution of initial structures differently due to molecular size and bonding. Consider the examples discussed so far, chemical intuition would suggest that experimental temperature will have a larger effect on both the SO<sub>3</sub> and para-methyl phenolate anions than the vinyl-phenolate anion due to size and rigidity of the molecular system. Furthermore, one might expect different dependencies on temperature to arise for the two direct detachment channels of the para-phenolate anions, based on the relative localisation of the Dyson orbitals that describe the two electron loss channels (see Figure 1).

In order to investigate the effect of temperature on modelling PADs, the equilibrium geometries of the SO<sub>3</sub>, para-methyl and para-vinyl phenolate anions were displaced by a temperature dependent Wigner distribution. For each temperature, a sample of ten displaced geometries were calculated and the average compared to the equilibrium geometry. Plots showing the modelled PADs for all ten displaced geometries for the different direct detachment channels are shown for each temperature in the Supporting Information. Note that a sample size of ten geometries is small, however, inspection of the variation in the modelled PADs (see Supporting Information Figures SI2-6) clearly demonstrated that even with a restricted sample size, the effect of temperature modulated displacements is clear. The purpose of this section is a proof-of-concept showcase, rather than a thorough investigation of temperature on the modelled PADs, which will be the focus of a future study. The results are shown in Figures 4. For all anions, the PADs were modelled using B3LYP/aug-cc-pVTZ orbital densities to represent the Dyson orbitals.

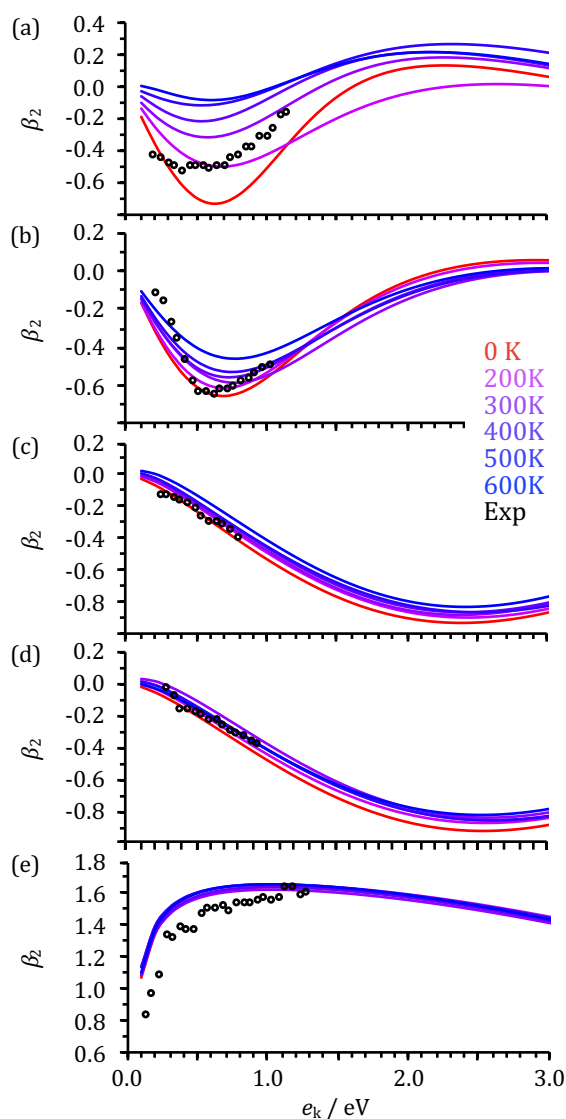


Figure 4 The effect of temperature mediated distortion from the equilibrium geometry of the parent anions on the modelled PADs for the  $D_0$  channel of para-methyl phenolate (a) and para-vinyl phenolate (b), the  $D_1$  channel of para-methyl phenolate (c) and para-vinyl phenolate (d) and the  $S_0$  channel of the  $SO_3$  anion (e). Legend is shown inset.

Overall, the variations in modelled PADs with changing temperature were different across the five direct detachment channels, Figure 4 (a) - (e). However, for all cases except the  $SO_3$  anion, the 0 K PAD is significantly different than the finite temperature PAD. Increasing the internal temperature of the molecular anion causes greater geometric perturbations away from the equilibrium geometry. While more dramatic changes to nuclear configurations can lead to

dramatic changes in electron density of the orbital, there are important distinctions between when and how this might occur.

As expected, changing nuclear structure has very little effect on the distribution of electron density of the  $D_1$  channel of the para-phenolates, Figure 4(c) and (d). The orbital density of this electron loss channel is localised to the oxygen atom of the phenolate moiety, and as such the temperature dependence for this channel is extremely low.

However, between the two para-phenolates there is a marked difference in variation of modelled PADs of the  $D_0$  channel with increasing temperature; methyl-phenolate shows a much greater dependence than vinyl-phenolate, Figure 4(a) and (b), respectively. Geometric displacements at even 200 K cause a large change from the modelled PADs of the equilibrium geometry of para-methyl phenolate, giving far better quantitative agreement with the experimental results. The difference in results between para-methyl and para-vinyl phenolate can be understood when considering the relative degrees of freedom of the two systems. The extension of the  $\pi$ -system in para-vinyl phenolate increases the rigidity of the nuclear framework, requiring more internal energy to cause geometric disruptions that would lead to substantial changes in electron density. Pleasingly, this finding offers an explanation as to the offset observed between the modelled PADs of the equilibrium geometry of para-methyl phenolate and the experimental findings. The experimental temperature of the anions is  $\sim 300$  K, in good agreement with Figure 4 (a). This preliminary finding indicates a route for extracting the internal temperature of molecular anions, although we note that our study used a limited number of Wigner displaced geometries.

The final  $S_0$  direct detachment channel of the  $SO_3$  anion, is perhaps the least intuitive finding. Figure 4(e) shows very little temperature dependence despite the molecule being small and having a highly delocalised orbital density. Further investigation of the individual displaced geometries for each of the temperatures (as shown in the Supporting Information

Figure SI6), can offer some insight. As the temperature increases, so too does the deviation from the modelled PAD of equilibrium geometry, however, this occurs in an entirely symmetric fashion. That is to say, distortions resulting in a complete loss of symmetry lead to a lowering in anisotropy, while distortions that preserve symmetry led to an equal but opposite increase in anisotropy. The overall result leads to almost indistinguishable changes in PADs with increasing temperature.

### **Further Considerations**

In principle, advances in accurate theoretical modelling of electronically excited states of anions that are embedded in the continuum should extend the feasibility of this analysis to metastable states. To the best of the authors knowledge, a benchmark study of the PADs from a metastable state does not yet exist, rather this remains a fascinating open challenge. From experimental studies, it has been demonstrated that the PADs often show far greater sensitivity to the onset of resonance channels than the energy spectra. Thus far, information about resonance electron loss channels has only been inferred. Given the ubiquity of resonances in nature, exploiting the Dyson orbital approach to model and interpret the PADs represents an area of great promise for future work. Extension of the Dyson orbital approach would allow confident interpretation of the character of the state, including the balance of the localised molecular orbital component and the delocalised continuum component.

### **Conclusions**

The aim of this study is two-fold; first, to demonstrate the power of the information encoded in the PADs complementary to the kinetic energy spectrum, and second, to provide a framework to encourage quantitative modelling of the PADs. We have presented an investigation and discussion of routes to designing calculations that will balance the

computational cost and accuracy of modelling PADs for larger molecular anions, considering pitfalls that may be overlooked in both the experimental conditions and computational approach. The key findings are:

(1) In order to accurately describe the photodetachment orbital of anions, it is advised to use augmented functions; our results demonstrate that elimination of this parameter in the basis set leads to deviations between trends in modelled and experimental anisotropy.

(2) While the Dyson orbitals calculated by the EOM-XX-CCSD methods are mathematically rigorous, for direct detachment channels that are well-described by a single electron transition, we have shown that canonical orbitals obtained from cheaper electronic structure methods can also yield accurate modelled PADs. Specifically, DFT orbitals provide an accurate description of the photodetachment orbital for the direct detachment channels studied.

(3) Temperature dependent displacements from the calculated equilibrium geometry can have an important impact on the computed PADs and should be accounted for in cases where the orbital density is sensitive to small nuclear displacements. Indeed, the 0 K PAD is generally not a quantitatively accurate description of an experimental PAD at 300 K. For highly localised orbitals, such as the  $D_1$  channel of the para-phenolates, geometric distortion has a negligible effect on the modelled PADs. However, for highly delocalised orbitals, such as the  $D_0$  channel of the para-phenolates, changes to nuclear structure cause much larger changes to the electronic structure, and therefore the modelled PADs. Rigid molecules require larger internal temperatures to cause the extent of distortion needed to affect the orbital density, and therefore the PADs. Molecules with larger degrees of internal freedom, even simply the addition of a methyl-group in the case of para-methyl phenolate, see fluctuations away from the modelled PADs of the equilibrium geometry at lower temperatures. Simply put, at lower temperatures  $\sim 200 - 300$  K, one should look to displacement in nuclear geometry away from the equilibrium geometry to explain discrepancies between experimental and modelled PADs. One can verify

this as the source of unexpected or deviating experimental PADs through distortion along low energy modes, using these displaced structures to model the changing PADs. Such an investigation can be conducted using a less expensive electronic structure method, such as DFT.

(4) Based on the above findings, there is also a clear need for an accurate equilibrium geometry, and so compromises in computational cost when obtaining this starting structure should be avoided. As such, molecular anions with shallow potential energy surfaces represent a challenge.

Taking the above points into consideration, it is now possible to predict in a semi-quantitative manner the expected PADs for direct one-electron photodetachment channels of polyatomic anions. We have demonstrated and benchmarked the importance of a number of parameters to ensure that physically meaningful PADs can be calculated and interpreted for large molecular anions. Finally, we have provided insight into the effect of experimental temperature on the geometry of delocalised canonical orbitals, providing an explanation for deviations based on experimental conditions.

#### AUTHOR INFORMATION

\*Corresponding Author: [csanstoter@gmail.com](mailto:csanstoter@gmail.com). The authors declare no competing financial interests.

#### ACKNOWLEDGMENT

This work was supported by the University of Durham. CSA wishes to thank Pratip Chakraborty for his guidance with Newton-X, and Spiridoula Matsika for use of the cluster to run these calculations. This work was conducted using the resources of the iOpenShell Center for Computational Studies of Electronic Structure and Spectroscopy of Open-Shell and

Electronically Excited Species (<http://iopshell.usc.edu>). Finally, the authors would like to thank the two referees for their insightful and constructive comments.

## References

- (1) Neumark, D. M. Time-Resolved Spectroscopy of Molecules and Clusters. *Annual Review of Physical Chemistry* **2001**, *52* (1), 255–277. <https://doi.org/10.1146/annurev.physchem.52.1.255>.
- (2) Neumark, D. M. Probing Chemical Dynamics with Negative Ions. *The Journal of Chemical Physics* **2006**, *125* (13), 132303. <https://doi.org/10.1063/1.2216709>.
- (3) Anstöter, C. S.; Bull, J. N.; Verlet, J. R. R. Ultrafast Dynamics of Temporary Anions Probed through the Prism of Photodetachment. *International Reviews in Physical Chemistry* **2016**, *35*, 509–538. <https://doi.org/10.1080/0144235X.2016.1203522>.
- (4) Arnold, D. W.; Bradforth, S. E.; Kitsopoulos, T. N.; Neumark, D. M. Vibrationally Resolved Spectra of C<sub>2</sub>–C<sub>11</sub> by Anion Photoelectron Spectroscopy. *J. Chem. Phys.* **1991**, *95* (12), 8753–8764. <https://doi.org/10.1063/1.461211>.
- (5) Hendricks, J. H.; Lyapustina, S. A.; de Clercq, H. L.; Snodgrass, J. T.; Bowen, K. H. Dipole Bound, Nucleic Acid Base Anions Studied via Negative Ion Photoelectron Spectroscopy. *The Journal of Chemical Physics* **1996**, *104* (19), 7788–7791. <https://doi.org/10.1063/1.471482>.
- (6) Wenthold, P. G.; Lineberger, W. C. Negative Ion Photoelectron Spectroscopy Studies of Organic Reactive Intermediates. *Accounts of Chemical Research* **1999**, *32* (7), 597–604. <https://doi.org/10.1021/ar960121x>.
- (7) Bailey, C. G.; Dessent, C. E. H.; Johnson, M. A.; Bowen, K. H. Vibronic Effects in the Photon Energy-dependent Photoelectron Spectra of the CH<sub>3</sub>CN<sup>−</sup> Dipole-bound Anion; 1996. <https://doi.org/10.1063/1.471415>.
- (8) Schiedt, J.; Weinkauff, R. Resonant Photodetachment via Shape and Feshbach Resonances: P-Benzoquinone Anions as a Model System. *The Journal of Chemical Physics* **1999**, *110* (1), 304–314. <https://doi.org/10.1063/1.478066>.
- (9) Stolow, A.; Bragg, A. E.; Neumark, D. M. Femtosecond Time-Resolved Photoelectron Spectroscopy. *Chemical Reviews* **2004**, *104* (4), 1719–1758. <https://doi.org/10.1021/cr020683w>.
- (10) Neumark, D. M. Probing the Transition State with Negative Ion Photodetachment: Experiment and Theory. *Phys. Chem. Chem. Phys.* **2005**, *7* (3), 433. <https://doi.org/10.1039/b417886f>.
- (11) Sanov, A.; Mabbs, R. Photoelectron Imaging of Negative Ions. *International Reviews in Physical Chemistry* **2008**, *27* (1), 53–85. <https://doi.org/10.1080/01442350701786512>.
- (12) Neumark, D. M. Slow Electron Velocity-Map Imaging of Negative Ions: Applications to Spectroscopy and Dynamics. *The Journal of Physical Chemistry A* **2008**, *112* (51), 13287–13301. <https://doi.org/10.1021/jp807182q>.
- (13) Kunin, A.; Li, W.-L.; Neumark, D. M. Dynamics of Electron Attachment and Photodissociation in Iodide-Uracil-Water Clusters via Time-Resolved Photoelectron Imaging. *J. Chem. Phys.* **2018**, *149* (8), 084301. <https://doi.org/10.1063/1.5040673>.
- (14) Wang, L.-S. Perspective: Electrospray Photoelectron Spectroscopy: From Multiply-Charged Anions to Ultracold Anions. *The Journal of Chemical Physics* **2015**, *143* (4), 040901. <https://doi.org/10.1063/1.4927086>.

- (15) Bull, J. N.; West, C. W.; Verlet, J. R. R. On the Formation of Anions: Frequency-, Angle-, and Time-Resolved Photoelectron Imaging of the Menadione Radical Anion. *Chem. Sci.* **2015**, *6* (2), 1578–1589. <https://doi.org/10.1039/C4SC03491K>.
- (16) Rogers, J. P.; Anstöter, C. S.; Verlet, J. R. R. Ultrafast Dynamics of Low-Energy Electron Attachment via a Non-Valence Correlation-Bound State. *Nature Chemistry* **2018**, *10* (3), 341–346. <https://doi.org/10.1038/nchem.2912>.
- (17) Bochenkova, A. V.; Mooney, C. R. S.; Parkes, M. A.; Woodhouse, J. L.; Zhang, L.; Lewin, R.; Ward, J. M.; Hailes, H. C.; Andersen, L. H.; Fielding, H. H. Mechanism of Resonant Electron Emission from the Deprotonated GFP Chromophore and Its Biomimetics. *Chem. Sci.* **2017**, *8* (4), 3154–3163. <https://doi.org/10.1039/C6SC05529J>.
- (18) Cooper, J.; Zare, R. N. Angular Distribution of Photoelectrons. *The Journal of Chemical Physics* **1968**, *48* (2), 942–943. <https://doi.org/10.1063/1.1668742>.
- (19) Reid, K. L. Photoelectron Angular Distributions. *Annual Review of Physical Chemistry* **2003**, *54* (1), 397–424. <https://doi.org/10.1146/annurev.physchem.54.011002.103814>.
- (20) Sanov, A. Laboratory-Frame Photoelectron Angular Distributions in Anion Photodetachment: Insight into Electronic Structure and Intermolecular Interactions. *Annual Review of Physical Chemistry* **2014**, *65* (1), 341–363. <https://doi.org/10.1146/annurev-physchem-040513-103656>.
- (21) Mabbs, R.; Grumbling, E. R.; Pichugin, K.; Sanov, A. Photoelectron Imaging: An Experimental Window into Electronic Structure. *Chemical Society reviews* **2009**, *38* (8), 2169–2177. <https://doi.org/10.1039/b815748k>.
- (22) Khuseynov, D.; Blackstone, C. C.; Culberson, L. M.; Sanov, A. Photoelectron Angular Distributions for States of Any Mixed Character: An Experiment-Friendly Model for Atomic, Molecular, and Cluster Anions. *The Journal of Chemical Physics* **2014**, *141* (12), 124312. <https://doi.org/10.1063/1.4896241>.
- (23) Culberson, L. M.; Blackstone, C. C.; Sanov, A. Photoelectron Angular Distributions of Pyridinide: A Benchmark Application of the Mixed s–p Model to a Truly Polyatomic Anion. *J. Phys. Chem. A* **2013**, *117* (46), 11760–11765. <https://doi.org/10.1021/jp402507v>.
- (24) Laws, B. A.; Gibson, S. T.; Lewis, B. R.; Field, R. W. The Dicarboxyl Bonding Puzzle Viewed with Photoelectron Imaging. *Nat Commun* **2019**, *10* (1), 5199. <https://doi.org/10.1038/s41467-019-13039-y>.
- (25) Blackstone, C. C.; Wallace, A. A.; Sanov, A. Photoelectron Angular Distributions in Photodetachment from Polarised *d*-like States: The Case of HO<sub>2</sub><sup>-</sup>. *Molecular Physics* **2021**, *119* (1–2), e1831636. <https://doi.org/10.1080/00268976.2020.1831636>.
- (26) Simons, J. Ejecting Electrons from Molecular Anions via Shine, Shake/Rattle, and Roll. *J. Phys. Chem. A* **2020**, *124* (42), 8778–8797. <https://doi.org/10.1021/acs.jpca.0c08016>.
- (27) Oana, C. M.; Krylov, A. I. Dyson Orbitals for Ionization from the Ground and Electronically Excited States within Equation-of-Motion Coupled-Cluster Formalism: Theory, Implementation, and Examples. *The Journal of Chemical Physics* **2007**, *127* (23), 234106. <https://doi.org/10.1063/1.2805393>.
- (28) Oana, C. M.; Krylov, A. I. Cross Sections and Photoelectron Angular Distributions in Photodetachment from Negative Ions Using Equation-of-Motion Coupled-Cluster Dyson Orbitals. *The Journal of Chemical Physics* **2009**, *131* (12), 124114. <https://doi.org/10.1063/1.3231143>.
- (29) Jagau, T.-C.; Krylov, A. I. Characterizing Metastable States beyond Energies and Lifetimes: Dyson Orbitals and Transition Dipole Moments. *The Journal of Chemical Physics* **2016**, *144* (5), 054113. <https://doi.org/10.1063/1.4940797>.

- (30) Moitra, T.; Ponzi, A.; Koch, H.; Coriani, S.; Decleva, P. Accurate Description of Photoionization Dynamical Parameters. *J. Phys. Chem. Lett.* **2020**, *11* (13), 5330–5337. <https://doi.org/10.1021/acs.jpcllett.0c01337>.
- (31) Pickup, B. T. On the Theory of Fast Photoionization Processes. *Chemical Physics* **1977**, *19* (2), 193–208. [https://doi.org/10.1016/0301-0104\(77\)85131-8](https://doi.org/10.1016/0301-0104(77)85131-8).
- (32) Deleuze, M.; Pickup, B. T.; Delhalle, J. Plane Wave and Orthogonalized Plane Wave Many-Body Green's Function Calculations of Photoionization Intensities. *Molecular Physics* **1994**, *83* (4), 655–686. <https://doi.org/10.1080/00268979400101501>.
- (33) McWeeny, R.; Pickup, B. T. Quantum Theory of Molecular Electronic Structure. *Reports on Progress in Physics* **1980**, *43* (9), 1065–1144. <https://doi.org/10.1088/0034-4885/43/9/001>.
- (34) Dill, D. Fixed-Molecule Photoelectron Angular Distributions. *The Journal of Chemical Physics* **1976**, *65* (3), 1130–1133. <https://doi.org/10.1063/1.433187>.
- (35) Gozem, S.; Seidel, R.; Hergenhan, U.; Lugovoy, E.; Abel, B.; Winter, B.; Krylov, A. I.; Bradforth, S. E. Probing the Electronic Structure of Bulk Water at the Molecular Length Scale with Angle-Resolved Photoelectron Spectroscopy. *J. Phys. Chem. Lett.* **2020**, *11* (13), 5162–5170. <https://doi.org/10.1021/acs.jpcllett.0c00968>.
- (36) Jagau, T.-C.; Dao, D. B.; Holtgrewe, N. S.; Krylov, A. I.; Mabbs, R. Same but Different: Dipole-Stabilized Shape Resonances in CuF – and AgF –. *The Journal of Physical Chemistry Letters* **2015**, *6* (14), 2786–2793. <https://doi.org/10.1021/acs.jpcllett.5b01174>.
- (37) Van Duzor, M.; Mbaiwa, F.; Wei, J.; Singh, T.; Mabbs, R.; Sanov, A.; Cavanagh, S. J.; Gibson, S. T.; Lewis, B. R.; Gascooke, J. R. Vibronic Coupling in the Superoxide Anion: The Vibrational Dependence of the Photoelectron Angular Distribution. *The Journal of Chemical Physics* **2010**, *133* (17), 174311. <https://doi.org/10.1063/1.3493349>.
- (38) Mabbs, R.; Pichugin, K.; Sanov, A. Dynamic Molecular Interferometer: Probe of Inversion Symmetry in I<sub>2</sub>– Photodissociation. *J. Chem. Phys.* **2005**, *123* (5), 054329. <https://doi.org/10.1063/1.1997131>.
- (39) Weichman, M. L.; DeVine, J. A.; Levine, D. S.; Kim, J. B.; Neumark, D. M. Isomer-Specific Vibronic Structure of the 9-, 1-, and 2-Anthracenyl Radicals via Slow Photoelectron Velocity-Map Imaging. *Proceedings of the National Academy of Sciences* **2016**, *113* (7), 1698–1705. <https://doi.org/10.1073/pnas.1520862113>.
- (40) Anstöter, C. S.; Dean, C. R.; Verlet, J. R. R. Sensitivity of Photoelectron Angular Distributions to Molecular Conformations of Anions. *The Journal of Physical Chemistry Letters* **2017**, *8* (10), 2268–2273. <https://doi.org/10.1021/acs.jpcllett.7b00726>.
- (41) Anstöter, C. S.; Verlet, J. R. R. Gas-Phase Synthesis and Characterisation of the Methyl-2,2-Dicyanoacetate Anion Using Photoelectron Imaging and Dipole-Bound State Autodetachment. *J. Phys. Chem. Lett.* **2020**, *11*, 6456–6462. <https://doi.org/10.1021/acs.jpcllett.0c02036>.
- (42) Anstöter, C. S.; Gartmann, T. E.; Stanley, L. H.; Bochenkova, A. V.; Verlet, J. R. R. Electronic Structure of the Para-Dinitrobenzene Radical Anion: A Combined 2D Photoelectron Imaging and Computational Study. *Physical Chemistry Chemical Physics* **2018**, *20*, 24019–24026. <https://doi.org/10.1039/c8cp04877k>.
- (43) Stanley, L. H.; Anstöter, C. S.; Verlet, J. R. R. Resonances of the Anthracenyl Anion Probed by Frequency-Resolved Photoelectron Imaging of Collision-Induced Dissociated Anthracene Carboxylic Acid. *Chemical Science* **2017**, *8* (4), 3054–3061. <https://doi.org/10.1039/c6sc05405f>.
- (44) Anstöter, C. S.; Curchod, B. F. E.; Verlet, J. R. R. Geometric and Electronic Structure Probed along the Isomerisation Coordinate of a Photoactive Yellow Protein

- Chromophore. *Nature Communications* **2020**, *11* (1), 2827.  
<https://doi.org/10.1038/s41467-020-16667-x>.
- (45) Woodhouse, J. L.; Henley, A.; Parkes, M. A.; Fielding, H. H. Photoelectron Imaging and Quantum Chemistry Study of Phenolate, Difluorophenolate, and Dimethoxyphenolate Anions. *J. Phys. Chem. A* **2019**, *123* (13), 2709–2718.  
<https://doi.org/10.1021/acs.jpca.8b11121>.
- (46) Gozem, S.; Krylov, A. I. *EzDyson*; 2016.
- (47) Gozem, S.; Gunina, A. O.; Ichino, T.; Osborn, D. L.; Stanton, J. F.; Krylov, A. I. Photoelectron Wave Function in Photoionization: Plane Wave or Coulomb Wave? *Journal of Physical Chemistry Letters* **2015**, *6* (22), 4532–4540.  
<https://doi.org/10.1021/acs.jpcclett.5b01891>.
- (48) Krylov, A. I. From Orbitals to Observables and Back. *J. Chem. Phys.* **2020**, *153* (8), 080901. <https://doi.org/10.1063/5.0018597>.
- (49) Gozem, S.; Krylov, A. I. The EzSpectra Suite: An Easy-to-Use Toolkit for Spectroscopy Modeling. *WIREs Comp. Mol. Sci.* **2021**, *In Press*.
- (50) Anstötter, C. S.; Verlet, J. R. R. Photoelectron Imaging of the SO<sub>3</sub> Anion: Vibrational Resolution in Photoelectron Angular Distributions\*. *Molecular Physics* **2021**, *119* (1–2), e1821921. <https://doi.org/10.1080/00268976.2020.1821921>.
- (51) Shao, Y.; Gan, Z.; Epifanovsky, E.; Gilbert, A. T. B.; Wormit, M.; Kussmann, J.; Lange, A. W.; Behn, A.; Deng, J.; Feng, X.; et. al. Advances in Molecular Quantum Chemistry Contained in the Q-Chem 4 Program Package. *Molecular Physics* **2015**, *113* (2), 184–215. <https://doi.org/10.1080/00268976.2014.952696>.
- (52) Becke, A. D. Density-Functional Thermochemistry. III. The Role of Exact Exchange. *The Journal of Chemical Physics* **1993**, *98* (7), 5648–5652.  
<https://doi.org/10.1063/1.464913>.
- (53) Yanai, T.; Tew, D. P.; Handy, N. C. A New Hybrid Exchange–Correlation Functional Using the Coulomb-Attenuating Method (CAM-B3LYP). *Chemical Physics Letters* **2004**, *393* (1–3), 51–57. <https://doi.org/10.1016/j.cplett.2004.06.011>.
- (54) Adamo, C.; Barone, V. Toward Reliable Density Functional Methods without Adjustable Parameters: The PBE0 Model. *J. Chem. Phys.* **1999**, *110* (13), 6158–6170.  
<https://doi.org/10.1063/1.478522>.
- (55) Clark, T.; Chandrasekhar, J.; Spitznagel, G. W.; Schleyer, P. V. R. Efficient Diffuse Function-Augmented Basis Sets for Anion Calculations. III. The 3-21+G Basis Set for First-Row Elements, Li-F. *J. Comput. Chem.* **1983**, *4* (3), 294–301.  
<https://doi.org/10.1002/jcc.540040303>.
- (56) Dunning, T. H. Gaussian Basis Sets for Use in Correlated Molecular Calculations. I. The Atoms Boron through Neon and Hydrogen. *The Journal of Chemical Physics* **1989**, *90* (2), 1007–1023. <https://doi.org/10.1063/1.456153>.
- (57) Barbatti, M.; Ruckebauer, M.; Plasser, F.; Pittner, J.; Granucci, G.; Persico, M.; Lischka, H. Newton-X: A Surface-Hopping Program for Nonadiabatic Molecular Dynamics: Newton-X. *WIREs Comput Mol Sci* **2014**, *4* (1), 26–33.  
<https://doi.org/10.1002/wcms.1158>.
- (58) Barbatti, M.; Granucci, G.; Ruckebauer, M.; Plasser, F.; Crespo-Otero, R.; Pittner, J.; Persico, M.; Lischka, H. *NEWTON-X: A Package for Newtonian Dynamics Close to the Crossing Seam (v. 2.2)*; 2018.
- (59) Dodson, L. G.; Savee, J. D.; Gozem, S.; Shen, L.; Krylov, A. I.; Taatjes, C. A.; Osborn, D. L.; Okumura, M. Vacuum Ultraviolet Photoionization Cross Section of the Hydroxyl Radical. *J. Chem. Phys.* **2018**, *148* (18), 184302. <https://doi.org/10.1063/1.5024249>.